Applied Catalysis B: Environmental 156–157 (2014) 84–93

Contents lists available at ScienceDirect

Applied Catalysis B: Environmental

journal homepage: www.elsevier.com/locate/apcatb

Hydrogen production by catalytic decomposition of methane over Ni-Cu-Co alloy particles

Aik Chong Lua**, Hong Yan Wang*

School of Mechanical and Aerospace Engineering, Nanyang Technological University, 50 Nanyang Avenue, Singapore 639798, Republic of Singapore

ARTICLE INFO

Article history:
Received 9 July 2013
Received in revised form 21 February 2014
Accepted 26 February 2014
Available online 5 March 2014

Keywords:
Nickel catalyst
Cobalt catalyst
Ni-Cu-Co alloy
Unsupported catalyst
Methane decomposition
Hydrogen production
Carbon nano-fibre

ABSTRACT

A series of Ni-Cu-Co alloy catalysts with different atomic compositions were prepared by the thermal decomposition of fibrous Ni-Cu-Co oxalate precursors in methane atmosphere. The resulting porous aggregates of Ni-Cu-Co alloy particles, with crystalline sizes ranging from 12.6 to 15.9 nm, showed good catalytic activities for methane decomposition in the temperature range from 650 to 775 °C. The percent composition of the constituent metals in the Ni-Cu-Co alloy catalyst was a dominant parameter that could affect the catalytic activity of the catalyst. When compared with the Ni-Cu alloy, the addition of cobalt was found to inhibit the quasi-liquid phenomenon effectively. With increasing cobalt content, the catalyst stability at higher temperature was improved but further continual increase of cobalt content led to phase separation as evidenced by the X-ray diffraction (XRD) patterns. The mechanism for the stabilizing effect of cobalt is discussed. The textural properties of the carbon nano-fibres were characterized by transmission electron microscopy and XRD.

1. Introduction

Presently, there is an increasing interest in using fuel cells as a mean to generate electricity. Fuel cells are highly efficient devices that produce electricity and heat by electrochemical oxidation of hydrogen and it is believed that in the near future, mass production of hydrogen will be possible on a large commercial scale. It is also generally believed that in the near to medium term, future hydrogen production will continue to rely on fossil fuels, primarily natural gas. However, the current viable method of hydrogen production has generated large quantities of CO_2 and CO. This necessitates the removal of these greenhouse gases which are known for contributing to global warming. Moreover, CO concentrations must be reduced to a few parts per million (ppm) to prevent poisoning of the electrocatalysts used in fuel cells [1–4]. For instance, phosphoric acid fuel cells, which are the most commercially developed fuel cells, do not tolerate CO concentrations above 1.5% [5]. The CO-free requirement of the hydrogen stream is even more stringent (ppm level) for the proton exchange membrane fuel cells. Therefore, in recent years, efficient, economical and environmentally friendly production of hydrogen is increasingly important and has attracted much research interests and activities.

Amongst many hydrogen production reactions, the catalytic decomposition of methane (CDM) (equation 1) has attracted widespread attention [6]. The major driving factor for the research activities on catalytic methane decomposition is the highly desirable products––CO_x-free hydrogen and carbon nanotube (CNT) or carbon nanofibre (CNF) instead of gaseous CO_x. This reaction will eliminate the need for CO_x separation and sequestration processes altogether. Compared with gaseous CO_x, the solid carbon is easier and safer to store. The CDM process coupled to a fuel cell facility is expected to provide a green approach to energy use. The by-product of the CDM process in the form of CNT or CNF is highly desirable as much progresses have been achieved for the applications of carbon nanomaterials in the area of nanocomposites and energy storage such as CNT/polymer composite [7,8], CNT/metal composite [9], water treatment [10], cathode catalysts for fuel cells [11] and supercapacitors [12]. Hence, the by-product of CDM will have potential applications depending on the quality.

The catalytic decomposition of methane is as follows:

$$CH_4 \rightarrow C + 2H_2 \quad \Delta = 75.6\,kJ/mol \tag{1}$$

Metallic nickel supported on textural promoters has been the most commonly used catalyst for methane decomposition due to its higher catalytic activity as compared with Co-based and Fe-based catalysts in the temperature range of 500–700 °C [13,14]. For

* Corresponding author. Tel.:+65 85060278.
** Corresponding author. Tel.: +65 67905535; fax: +65 67924062.
E-mail addresses: maclua@ntu.edu.sg (A.C. Lua), wanghongyan12@hotmail.com (H.Y. Wang).

http://dx.doi.org/10.1016/j.apcatb.2014.02.046
0926-3373/

supported nickel catalyst [15–19], it has been deduced that, with increasing temperature (e.g. 500 °C → 550 °C → 580 °C → 700 °C), the optimal particle domain size decreases (e.g. 60–100 nm → 30–40 nm → 34 nm → 10–20 nm). This trend is probably due to the delicate balance between the methane decomposition rate and the carbon diffusion rate. Particle size has a major influence on both reaction rates. It is likely that a self-organizing system can regulate the particle size to adapt to the reaction conditions. Therefore, support materials, such as Al_2O_3, SiO_2 and MgO, are commonly used to control the catalyst particle size and dispersion by physical interactions (porous support) or chemical interaction (charge transfer effect) [20]. It was reported that a 40% Ni/SiO_2 catalyst could lead to a carbon yield as high as 491 gC/gNi during methane decomposition at 500 °C [17]. The 15Ni-3Cu-2Al_2O_3 catalyst prepared from a hydrotalcite-like precursor could produce a high carbon yield of 630.6 gC/gNi at 600 °C [21]. It was also found that supported Ni-Cu on niobium oxide led to a carbon yield of up to 743 g C/gNi at 600 °C [22]. However, it is important to highlight that the thermal decomposition of methane over supported catalysts may lead to the formation of traceable CO via the reaction of the carbonaceous residues with the oxygen in the support, as in SiO_2 and Al_2O_3 [5,23,24]. Furthermore, with a supported catalyst, the strong binding of the catalyst and the carbon nanotubes (CNTs) to the support material, like SiO_2 and Al_2O_3, causes difficulties in cleaning the CNTs to make them a practical by-product. Hence, unsupported nickel catalyst could provide easy recovery of the catalyst and a convenient way for purifying the CNTs by leaching the metal catalyst with a mild acid solution [25]. For example, CNTs can be purified by dispersing them in nitric acid solution [26–29] or hydrochloric acid solution [30]. The metallic nickel catalyst will be dissolved and the solution can be separated from the CNTs by vacuum filtration. Hence, the CNTs will be recovered as the residue. By adjusting the pH value, the nickel ion solution can be recovered and used for preparing nickel oxalate, which is the precursor for unsupported nickel catalyst.

A few successful attempts were made to synthesize unsupported nickel catalyst for the methane decomposition reaction [6,25,31]. Li et al. [25] prepared nickel oxide with controlled crystallite size and fibrous morphology through precipitation of nickel oxide from nickel acetate with the mediation of ethylene glycol. The nickel oxide showed good catalytic activity with carbon yields of 354–398 gC/gNi.

Recently, the authors reported that unsupported nickel particles or Ni-Cu alloy particles, which showed promising catalytic activities, were simply prepared by the decomposition of nickel oxalate or Ni-Cu oxalate in a certain atmosphere (methane, nitrogen or air) [19,32]. The final amounts of carbon produced by methane decomposition at 550, 525 and 500 °C were 217 gC/gNi, 282 gC/gNi and 302 gC/gNi, respectively and it was found that collisions between two Ni catalyst particles or between Ni particles and CNFs may also lead to catalyst deactivation due to growth space limit [19]. Besides Ni element, supported Ni-Cu catalysts have also been widely studied [33–41] and a great improvement in the stability of the supported Ni-Cu was generally observed when compared with supported Ni catalyst. However, the occurrence of the quasi-liquid state catalyst was reported to be the main reason for catalyst deactivation under high temperatures, especially for Ni-Cu catalysts [32,34,36]. This could be attributed to the lower melting point of Cu. To continue the authors' earlier research which focused on the catalytic performance of a series of Ni-Cu alloy catalysts [32], cobalt was doped into the Ni-Cu agglomerates to increase the catalyst stability at high temperatures in this work. The objective of this study was to investigate the genesis of the phase composition and properties of Ni-Cu-Co alloy catalysts. The nominal and actual compositions of the Ni-Cu-Co catalyst are summarized in Table 1.The copper content in all the catalysts was kept at 25% which was the same as the Ni-Cu-3 sample.

Table 1
Compositions of different Ni-Cu-Co oxalate samples.

Sample	Ni/Co/Cu (nominal atomic ratio)	Ni/Co/Cu (analyzed by energy dispersive X-ray spectroscopy)
Ni-Cu-3	0.75/0/0.25	0.777/0/0.223
Ni-Cu-Co-1	0.7/0.05/0.25	0.743/0.054/0.202
Ni-Cu-Co-2	0.625/0.125/0.25	0.670/0.127/0.202
Ni-Cu-Co-3	0.5/0.25/0.25	0.536/0.239/0.225
Ni-Cu-Co-4	0.375/0.375/0.25	0.405/0.373/0.220
Ni-Cu-Co-5	0.25/0.5/0.25	0.269/0.502/0.228
Cu-Co	0/0.75/0.25	0/0.787/0.212

2. Experimental

2.1. Preparation of catalyst precursor

Ni-Cu-Co mixed oxalates were used as precursors for preparing the Ni-Cu-Co alloy particles. A series of mixed oxalates with different Ni/Co/Cu proportions were prepared by a precipitation method, followed by a hydrothermal process. In a typical procedure, certain amounts of $Ni(NO_3)_2{\cdot}6H_2O$, $Cu(NO_3)_2{\cdot}3H_2O$ and $Co(NO_3)_2{\cdot}6H_2O$ with a total metal ions of 9 mmol were dissolved in 30 ml of pure ethanol. The compositions of the six samples are listed in Table 1. A stoichiometric amount of oxalic acid, dissolved in 30 ml pure ethanol, was titrated to the above solution using a burette and was subjected to magnetic stirring for 30 min during and after titration. The light pink suspension was transferred into a 100 ml capacity Teflon-lined stainless steel autoclave and kept at 120 °C for 12 h. After cooling to room temperature, a purple solid precipitate was obtained by filtration and then thoroughly washed with distilled water. The resulting precipitate was dried at 80 °C in a vacuum oven.

2.2. Preparation of Ni-Cu-Co alloy catalyst

Alloy particles were synthesized by heating the prepared Ni-Cu-Co oxalate samples in a CH_4-N_2 mixture stream ($CH_4/N_2 = 1$) with a total flow rate of 25 ml/min. For the methane decomposition tests with the same amount of catalyst in each test, a fixed mass of Ni-Cu-Co oxalate (typically, 150 mg) was placed in the centre of a quartz tube reactor (ID 10 mm, length 800 mm) and the sample was supported on quartz wool. A K-type thermocouple covered with a quartz thermo-well was placed near the catalyst bed to detect the temperature of the catalyst bed. The reactor was vertically fitted in an electric furnace (Lenton, LTF/12/28/500). Ni-Cu-Co oxalates were dehydrated and decomposed into Ni-Cu-Co alloy by heating the oxalates up to 450 °C. Based on thermo-gravimetric analysis (TGA) under N_2 atmosphere, the mass of the oxalate sample (with an initial mass of 0.15 g) after dehydration and decomposition was found to be in the range of 0.0516 g to 0.0537 g, which could be considered as the fixed mass of catalyst used in these tests. In some tests in which the mass of metallic nickel content (i.e. 0.0404 g) in the catalysts was held constant and at the same time having the same atomic proportions (ratios) of the constituent metallic components as given in Table 1, the masses of the catalysts (based on TGA analysis) were as follows: Ni-Cu-Co-1: 0.0543 g, Ni-Cu-Co-2: 0.0604 g, Ni-Cu-Co-3 0.0754 g, Ni-Cu-Co-4 0.0998 and Ni-Cu-Co-5: 0.1502 g.

2.3. Methane decomposition reaction

When the metallic catalyst was formed in the quartz tube reactor, methane decomposition reaction commenced by increasing the

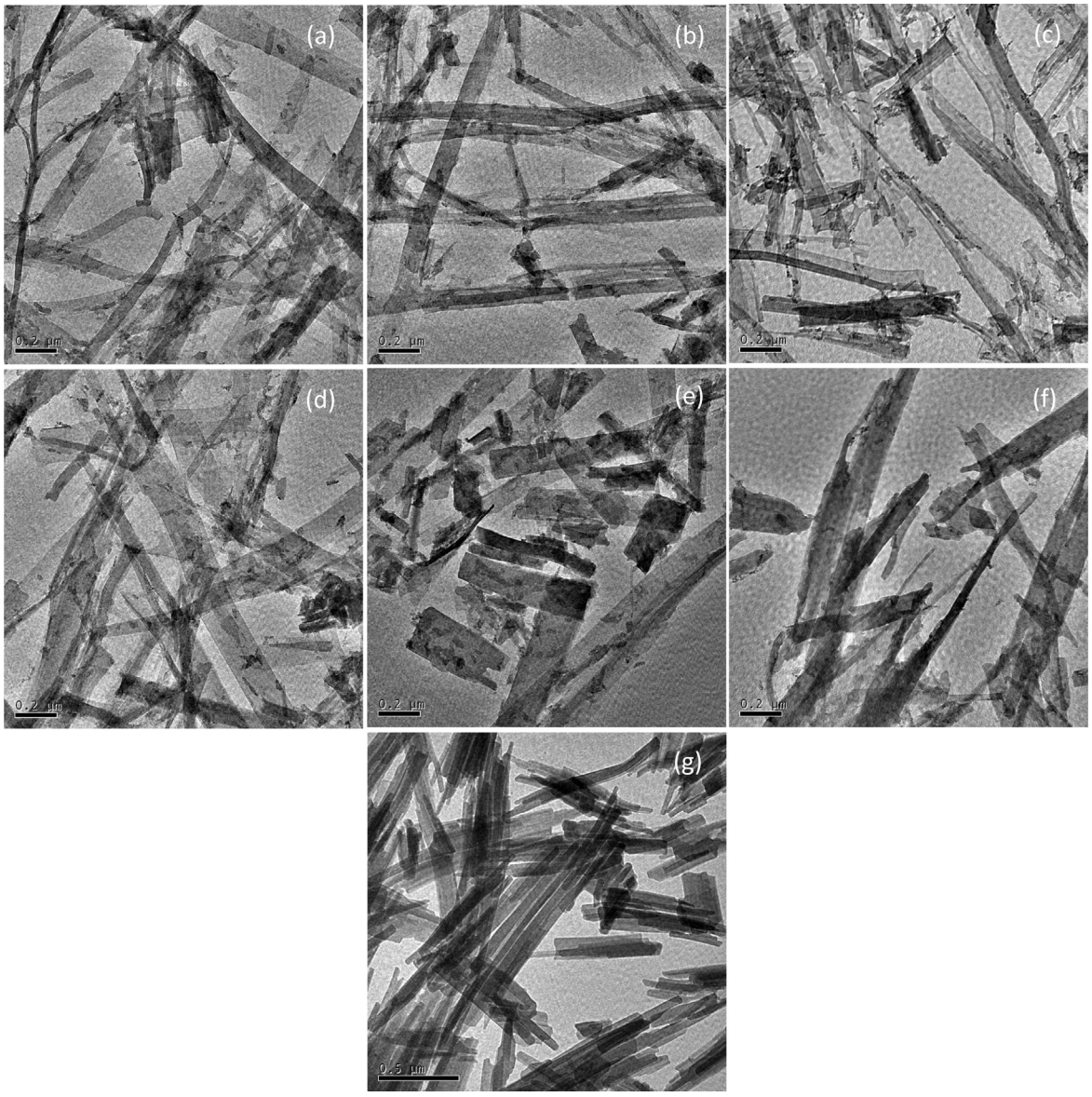

Fig. 1. TEM micrographs of Ni-Cu-Co oxalates, Co-Cu oxalate and pure cobalt oxalate: (a) Ni-Cu-Co-1, (b) Ni-Cu-Co-2, (c) Ni-Cu-Co-3, (d) Ni-Cu-Co-4, (e) Ni-Cu-Co-5, (f) Co-Cu and (g) Co.

furnace temperature to the desired reaction temperature and maintained for a certain period. CH_4-N_2 ($CH_4/N_2 = 0.25$) was used as the reaction gas with a total flow rate of 25 ml/min. The gases exiting the reactor were analyzed by a gas chromatograph (Agilent 6890 GC) equipped with a HP-molesieve column and a thermal conductivity detector using helium as the carrier gas. Prior to use, the gas chromatograph was carefully calibrated using fixed and certified compositions of CH_4-H_2-N_2 gas mixtures with uncertainties of 0.1–1%. The concentrations of hydrogen and methane at the reactor outlet were determined, which were based on these calibrated data and hence the methane conversion (defined as the number of moles of consumed methane divided by the initial number of moles of methane) was calculated. For all the samples, a series of reactions were carried out with a stepwise heating mode to obtain the general workable reaction temperature range. Several temperatures were selected: 500 °C, 600 °C, 650 °C, 700 °C, 750 °C, 800 °C and 850 °C. The reaction started at 500 °C. After a period of time (30 min), the temperature was increased at a rate of 10 °C/min to the next higher preset temperature of 600 °C. The stepwise heating continued until the conversion of methane was lower than that of the starting temperature.

2.4. Characterization of the fresh and used catalysts

In order to characterize the fresh metallic Ni-Cu-Co catalyst, a passivation treatment was conducted to avoid self-ignition of the nickel catalyst. After the metallic particle preparation phase (Section 2.2) had been completed, it was subsequently cooled down to ambient temperature in nitrogen atmosphere. Then, a slightly oxidizing O_2-N_2 mixture stream with 0.5% O_2 was allowed to flow through the prepared alloy particles for 1 h at room temperature before the sample was removed from the reactor.

TGA tests were carried out using a thermogravimetric analyzer (DTG-60H, Shimadzu) in a flowing nitrogen atmosphere with a heating rate of 5 °C/min. These TGA results provided the weight of the metallic catalyst after dehydration and decomposition of the oxalate precursor.

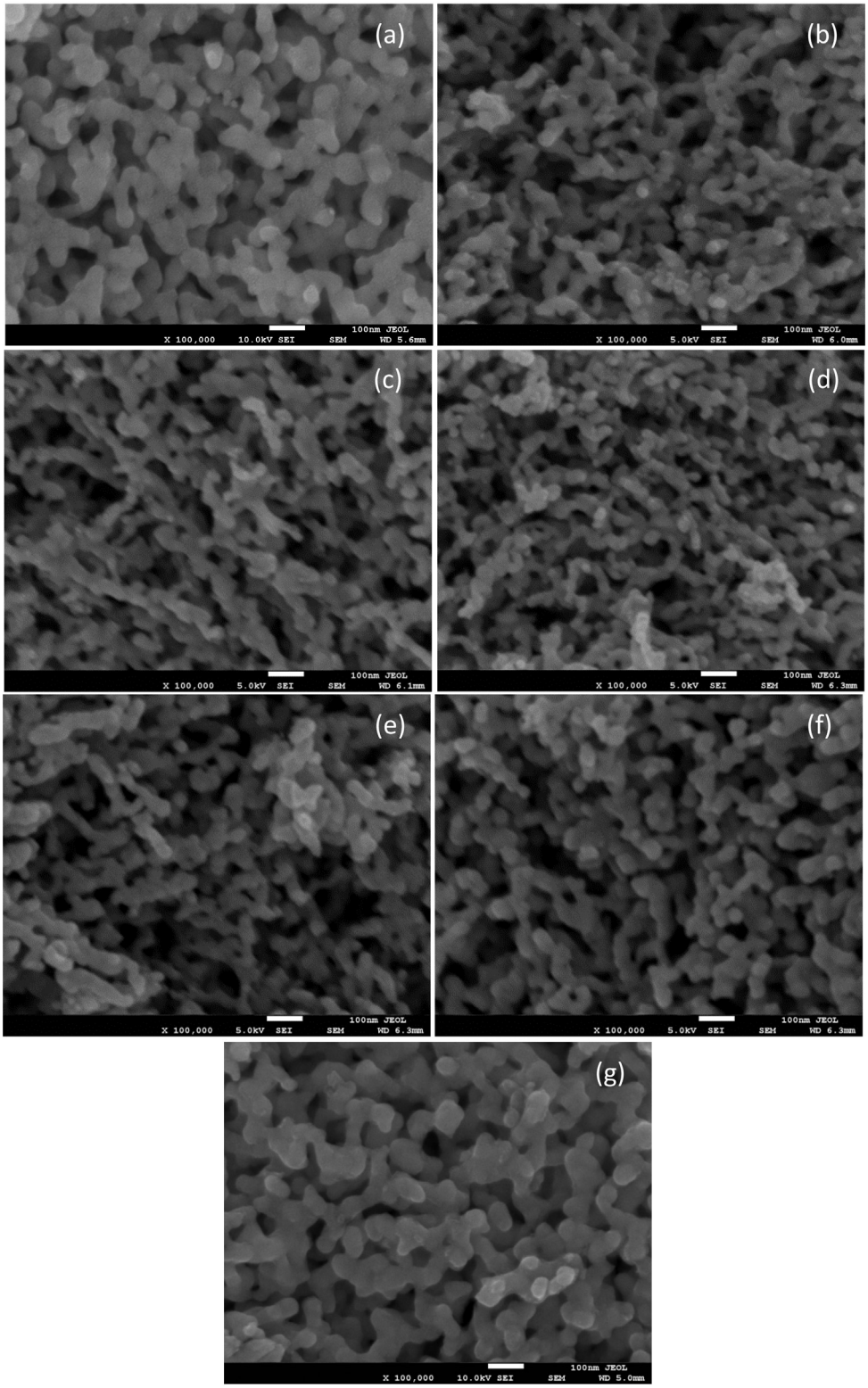

Fig. 2. FESEM micrographs of Ni-Cu, Co-Cu and Ni-Cu-Co alloys: (a) Ni-Cu-3, (b) Ni-Cu-Co-1, (c) Ni-Cu-Co-2, (d) Ni-Cu-Co-3, (e) Ni-Cu-Co-4, (f) Ni-Cu-Co-5, (g) Co-Cu.

Powder X-ray diffraction (XRD) patterns were measured by an X-ray instrument (Philips, PW1830) using CuKα (λ = 1.5406 Å) radiation at 30 kV and 20 mA, operating on a continuous scan mode. The XRD patterns were recorded in the scan range of 2θ = 10–90° at a scan rate of 1°/min. The mean crystallite sizes of Ni-Cu-Co alloy were calculated from the Scherrer equation [42], where the particle shape factor was taken as 0.9.

Field emission scanning electron microscopy (FESEM) was used to study the morphology and physical characteristics of the metallic Ni-Cu particle catalyst using a field emission scanning electron microscope (JEOL JSM-7600F).

A scanning electron microscope (SEM, JEOL JSM-5600LV) equipped with an energy dispersive X-ray spectroscopy (EDX) was used to analyze the composition of the alloy catalysts.

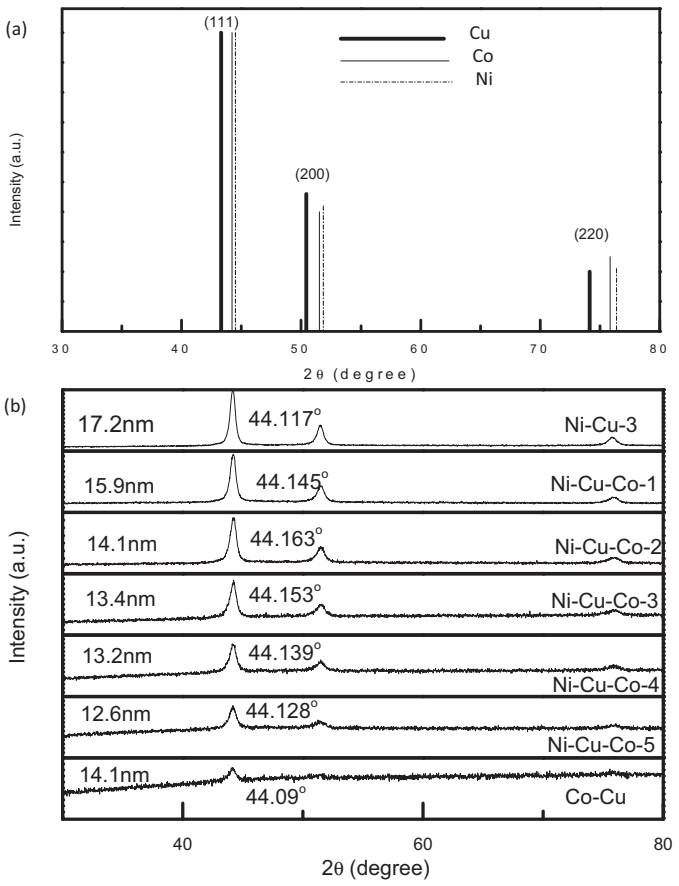

Fig. 3. XRD patterns of (a) reference and (b) Ni-Cu-Co alloys by reduction in methane gas stream.

Transmission electron microscopy (TEM) micrographs were also obtained using a transmission electron microscope (JEOL JEM 2010) with an operating voltage of 200 kV. Samples for the TEM analysis were prepared by drying sample particles in ethanol on carbon-coated copper grids.

3. Results and discussion

3.1. Characterization of the catalysts

Fig. 1 shows the morphologies of the Ni-Cu-Co oxalate hydrate samples as determined by TEM. When compared with the single or binary metal oxalate, the structures of the ternary oxalates tend to be more disordered and irregular. The ternary oxalates were made up of a mixture of wide and fine fibres. Similar to nickel oxalate, pure cobalt oxalate also showed fibre-like structures with smooth surfaces as shown in Fig. 1(g).

The morphological characteristics of the pristine Ni-Cu-Co alloy are shown in Fig. 2. All the samples appeared as large agglomerates of particles similar to the Ni-Cu series. The primary particles in close proximity had linked up and formed irregular shaped particles. When compared with the binary alloys Ni-Cu-3 (Fig. 2(a)) and Co-Cu (Fig. 2(g)), the ternary alloys showed smaller primary particle sizes.

The crystalline structures of the as-prepared Ni-Cu-Co alloy were characterized by XRD as shown in Fig. 3(b). For comparison purpose, the reference patterns of pure nickel, cobalt and copper are also shown in Fig. 3(a). All XRD patterns exhibit only one series of peaks corresponding to a face-centred-cubic (fcc) phase which is attributed to a Ni-Cu-Co solid solution [43,44] and are different

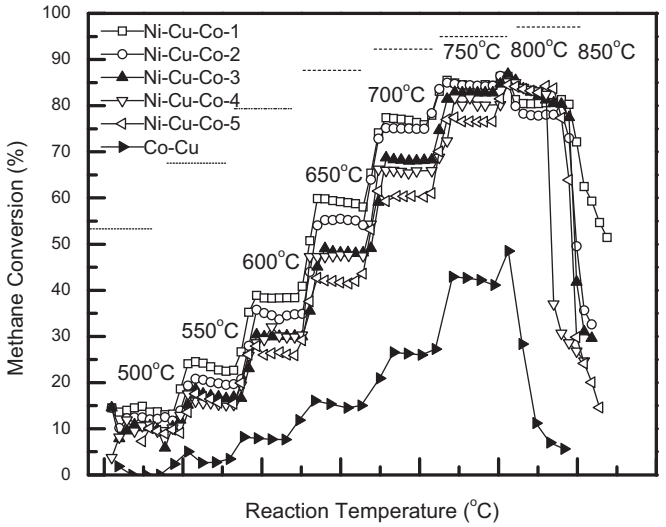

Fig. 4. Methane conversions during step-wise rising temperature reaction for Ni-Cu-Co alloy catalysts (dashed line—methane equilibrium conversion at different reaction temperatures).

from the respective individual diffractions of the physically mixed metallic samples [45]. There are no observable peaks in the XRD spectra that correspond to the spectrum of pure cobalt or copper. The diffraction peaks in the Ni-Cu-Co catalyst matched the (1 1 1), (2 0 0), (2 2 0) characteristics of a nickel or cobalt fcc structure but its 2θ value shifted slightly from that of nickel or cobalt as shown in Fig. 3(b). The 2θ values of pure Cu, Co and Ni are 43.298°, 44.217° and 44.508°, respectively. The shift in the 2θ values is due to the incorporation of cobalt and copper, suggesting the formation of a trimetallic alloy. The crystalline sizes were calculated and the domain sizes of Ni-Cu-Co alloy particles ranged from 12.6 to 15.9 nm.

3.2. Catalytic activity

Fig. 4 shows the methane conversions at different reaction temperatures for a series of nearly equal masses of Ni-Cu-Co alloy catalysts using a stepwise temperature heating mode. With specified raw material amounts, temperatures and the species of the system, the theoretical equilibrium methane conversions under different temperatures were calculated using the commercial HSC Chemistry software (©ChemSW Software, Inc.) [46] and these equilibrium limits were indicated as dashed lines. For all the samples, increasing temperature greatly increased the conversion rate as the process was an endothermic reaction. Without Ni, the Co-Cu sample yielded a much lower methane conversion when compared with samples which had Ni contents. Hence, nickel has a significantly greater catalytic activity than cobalt. All the ternary alloy samples exhibited high initial catalytic activities up to 750 °C. At 700 °C and below, the best conversion at each reaction temperature was obtained by the sample with the highest nickel content and the lowest cobalt content. However, at 750 °C, the differences in conversion among the ternary samples were insignificant. The maximum reaction temperature for these ternary alloy catalysts was 800 °C and beyond this temperature, a break-down in the catalyst was observed.

Figs. 5 and 6 show the performance of catalysts with time at constant reaction temperatures of 700 °C and 750 °C, respectively. In these experimental tests, the volume flow rate of the CH_4-N_2 gas stream feed was fixed at 25 ml/min (the CH_4 gas feed was 5 ml/min) and the mass of the alloy catalyst used in each test was about 0.05 g. In other words, the thickness of the catalyst layer in the quartz

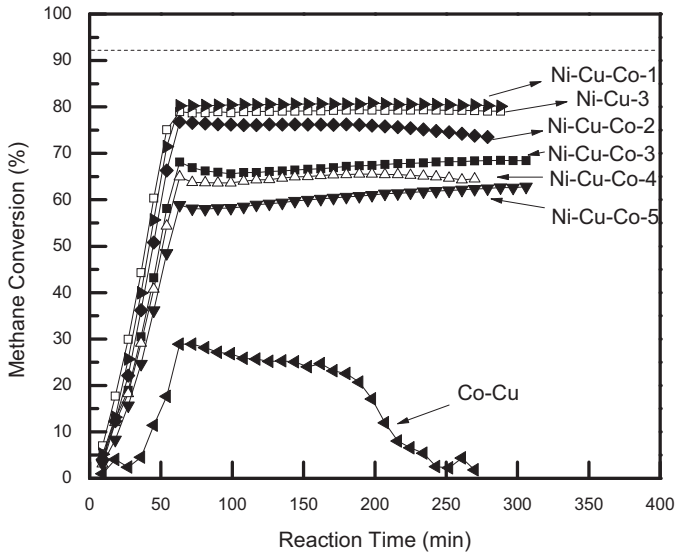

Fig. 5. Methane conversions using different catalysts at 700 °C (dashed line—methane equilibrium conversion at 700 °C).

tube reactor for all the tests remained approximately the same and hence the flow path length of the methane stream was being kept roughly constant. Thus, it could be assumed that the contact time of methane over the catalyst particles would be approximately the same for each test and that the contact time was not a varying parameter in these tests. At 700 °C, all the Ni-Cu-Co alloy samples and the Ni-Cu alloy sample provided and sustained good stability in methane conversions. Generally, a higher Ni content (as in Ni-Cu-Co-1 and Ni-Cu-3) produced higher methane conversion due to the good catalytic activity of nickel, with the best methane conversion of about 80% achieved by the catalyst sample Ni-Cu-Co-1. However, when the reaction temperature was increased to 750 °C, only samples with cobalt content of 12.5% and greater were able to provide stable catalytic activities over the test duration. At both reaction temperatures of 700 °C and 750 °C in Fig. 5 and Fig. 6, respectively, the Co-Cu catalyst, which had nearly the same mass as the Ni alloy catalysts, showed much lower methane conversion and significantly shorter stable reaction than all the Ni alloy catalysts.

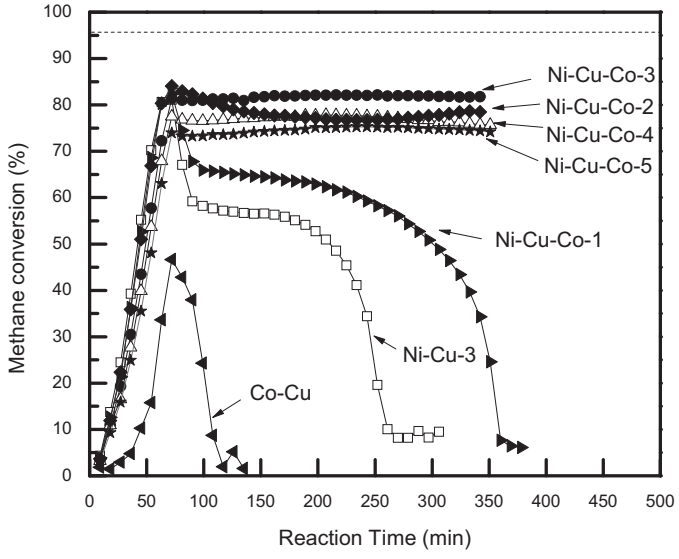

Fig. 6. Methane conversions using different catalysts at 750 °C (dashed line—methane equilibrium conversion at 750 °C).

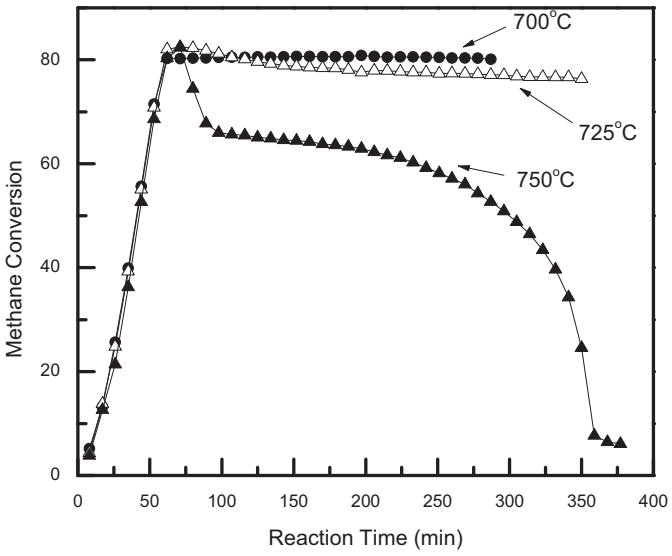

Fig. 7. Methane conversions using Ni-Cu-Co-1 at various reaction temperatures.

In order to determine the optimum operating reaction temperature for samples Ni-Cu-Co-1 and Ni-Cu-Co-3, which had shown to have good catalytic activities at 700 and 750 °C in Fig. 5 and Fig. 6, respectively, these samples were tested at various temperatures ranging from 650 to 775 °C as shown in Fig. 7 and Fig. 8. For both samples, their activities were greatly affected by temperature. An optimum temperature that yielded the best methane conversion did exist for each sample. For sample Ni-Cu-Co-1, the best methane conversion of about 82% with stable catalytic activity was obtained at 700 °C (Fig. 7) whereas for sample Ni-Cu-Co-3, the optimum reaction temperature was 750 °C with similar performance in methane conversion (Fig. 8). At a temperature higher by 25 °C (or 50 °C) than the optimum temperatures, a slow (or rapid) deactivation with time occurred.

To study the effect of varying amount of cobalt and copper with a fixed mass of nickel, a series of Ni-Cu-Co catalysts consisting of 0.0404 g of nickel and different percent compositions of nickel, cobalt and copper as given in Table 1 were used for the CDM reaction and the results are shown in Fig. 9. Comparing the results in Fig. 9 and Fig. 5 (the lowest and highest nickel masses were 0.0139 g

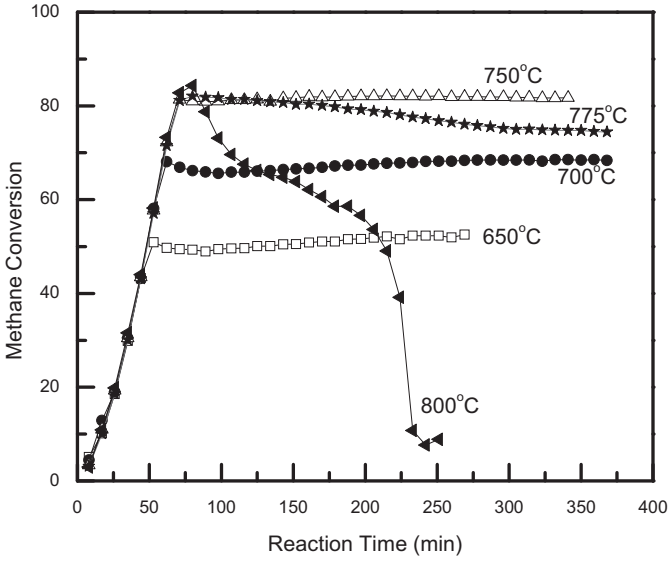

Fig. 8. Methane conversions using Ni-Cu-Co-3 at various reaction temperatures.

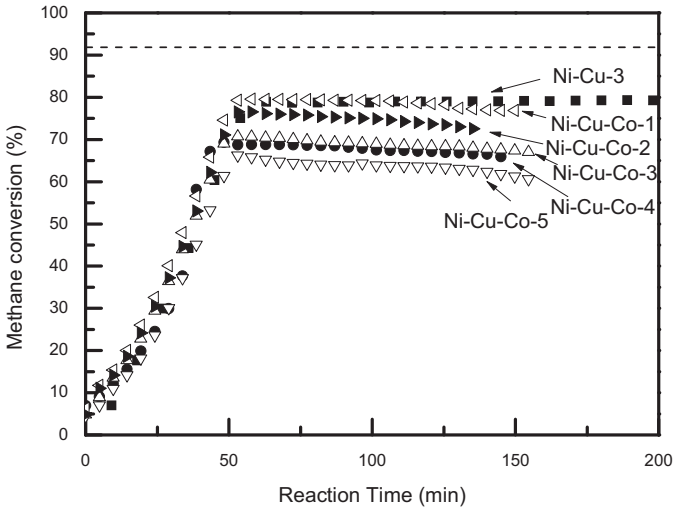

Fig. 9. Methane conversions using different catalysts with fixed Ni content at 700 °C (dashed line—methane equilibrium conversion at 700 °C).

(Ni-Cu-Co-5) and 0.0386 g (Ni-Cu-Co-1), respectively), all the catalysts showed fairly similar methane conversion yields except for Ni-Cu-Co-5 catalyst with 25% nickel content. (For the Ni-Cu-Co-5, the catalyst in Fig. 9 yielded about 4% higher in methane conversion than that in Fig. 5). Hence, these preliminary results showed that for nickel contents of 37.5% and higher in these Ni-Cu-Co catalysts (for the same order of magnitude of Ni mass) studied here, the actual mass of nickel percent in the catalyst was not the underlying factor that determined methane conversion yields but the percent composition of the constituent metals was a dominant parameter that would contribute to the catalytic activity of the Ni-Cu-Co alloy catalyst. It is surmised that the catalyst metal surface geometry and energetics may be changed with the incorporation of cobalt and copper into the Ni-Cu-Co alloy catalyst, leading to an increased energy barrier to methane conversion over the surface of the alloy catalyst [45,47]. Although the Ni-Cu-3 catalyst in Fig. 5 and Fig. 9 had almost the highest methane conversion yields and sustained stability with time, its stability deteriorated sharply with time when the CDM reaction temperature was increased to 750 °C as shown in Fig. 6.

Fig. 10 shows the XRD profiles of the spent catalysts after reactions at 700 °C and 750 °C. For most of the catalysts, nickel and copper existed in the alloy state after the reaction. However, for the catalysts with high cobalt content, such as Ni-Cu-Co-5 and Co-Cu, copper existed as a single phase as confirmed by the peak at 43.4° although these catalysts had formed alloys before the reaction as shown in Fig. 3. From the authors' earlier study [32], it was shown that nickel and copper could easily form an alloy and the alloy remained stable at reaction temperatures up to 750 °C. However, after cobalt was added and was predominant in the composition of the alloy, such as Ni-Cu-Co-5 and Co-Cu, phase separation was likely to occur at high reaction temperatures of 700 °C and greater.

After the reaction, the catalyst particles had sintered into much bigger particles as shown in Fig. 11 as compared with their corresponding pristine catalyst particles in Fig. 2. In the TEM micrographs of carbon deposited over Ni-Cu-Co catalysts in Fig. 11, no typical straight fibres were observed. After careful examination at high magnification, the "carbon fibres" were actually stacks of carbon fragments (Fig. 11(h)). They were joined so loosely that after the sample preparation process for the TEM analysis, the fibre structure was destroyed as shown in Fig. 11(d), (e) and (f). With increasing cobalt content (Fig. 11(a) to Fig. 11(e)), the geometrical shape of the catalyst also showed slight changes, from isometric morphologies with facets to spherical ones. Upon further increasing cobalt

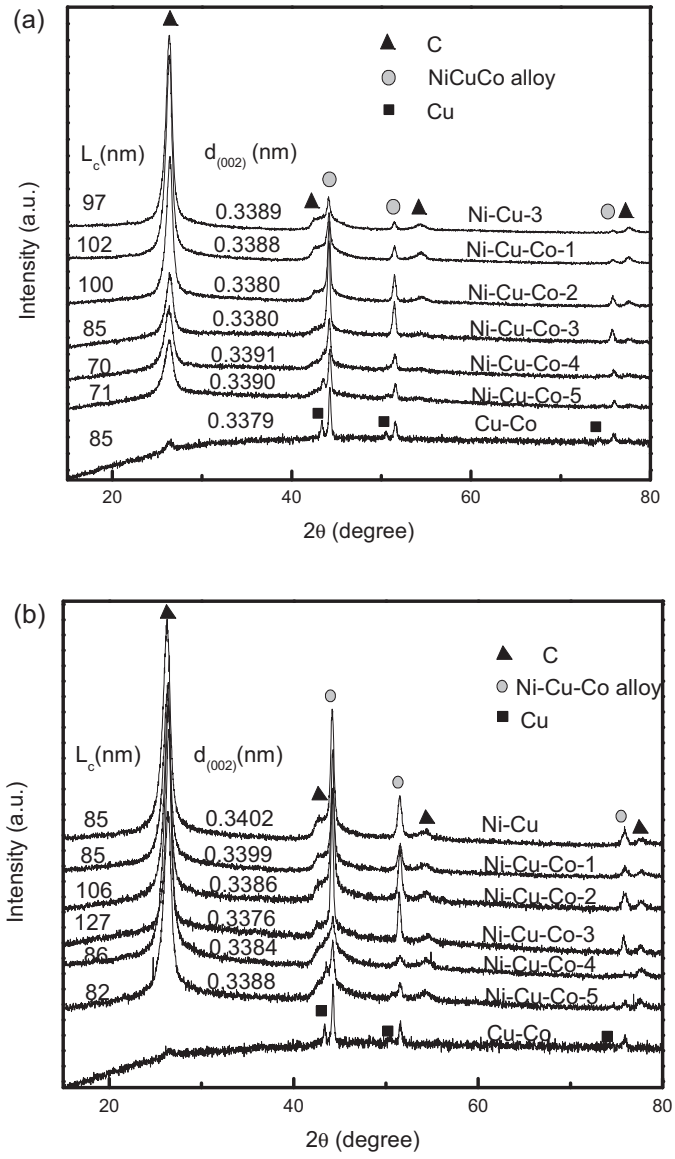

Fig. 10. XRD patterns of spent catalysts at different reaction temperatures: (a) 700 °C and (b) 750 °C.

content and decreasing nickel content, such as sample Ni-Cu-Co-5 (Fig. 11(f)) or Co-Cu (Fig. 11(g)), phase separation occurred as shown in Fig. 10. As observed from Fig. 11(g), the catalyst showed a rigid bulk followed by a conical tail, which was probably a copper phase, and separated from the Co-Cu alloy due to lower melting points and interfacial impact between carbon and liquid-state metal.

At a reaction temperature of 750 °C, samples with lower Co content became unstable. Two types of carbon were formed: multi-walled carbon nanotubes [48,49] (Fig. 12(a) and (b)) and carbon shells embedded with big catalyst particles (Fig. 12(c)). The catalyst particles underwent a dispersing process with increasing temperature in order to maintain the balance of a carbon migration cycle. Therefore, smaller Ni-Cu-Co alloy particles were formed as shown in Fig. 12(a). The liquid-like catalyst particle appeared with a tail which led to the formation of CNTs as shown in Fig. 12(b). The shape of the CNTs suggested that it was formed by jumping off the catalyst metal tips at regular time intervals over similar distances. Larger particles (>100 nm) were covered by carbon which led to abrupt deactivation (Fig. 12(c)). With increasing cobalt content, the particle size was not as crucial when compared with the particle

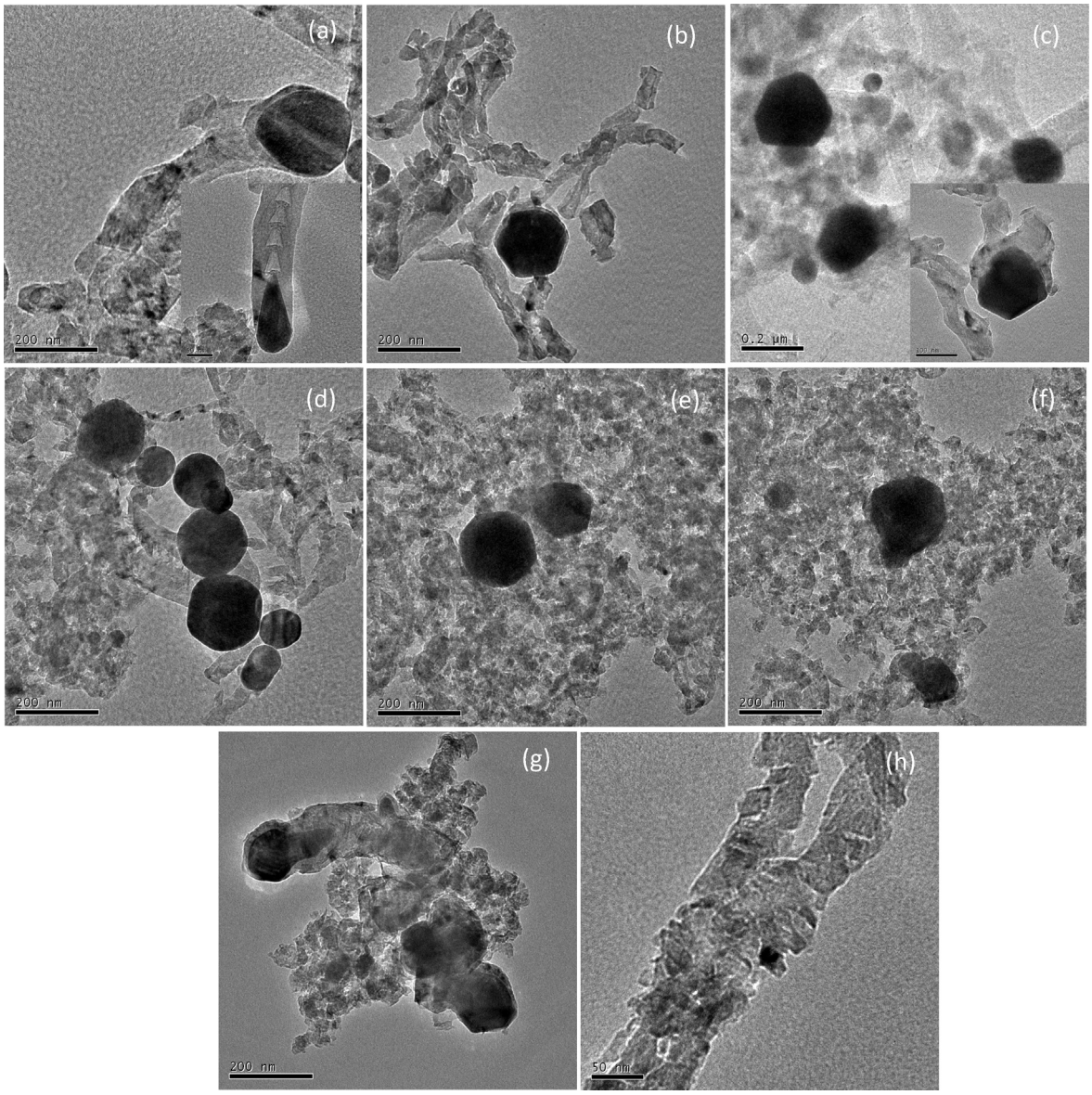

Fig. 11. TEM micrographs of spent catalysts: (a) Ni-Cu-3, (b) Ni-Cu-Co-1, (c) Ni-Cu-Co-2, (d) (h) Ni-Cu-Co-3, (e) Ni-Cu-Co-4, (f) Ni-Cu-Co-5, (g) Co-Cu at a reaction temperature of 700 °C.

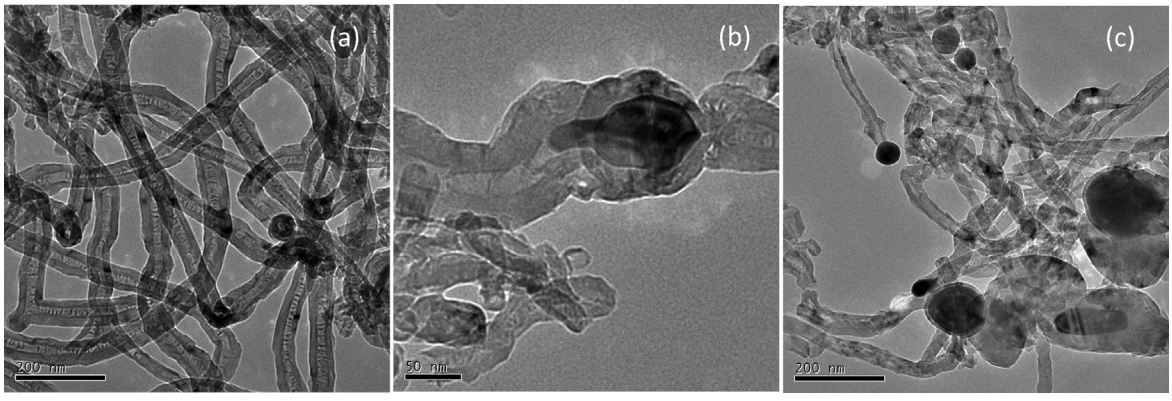

Fig. 12. TEM micrographs of spent catalyst Ni-Cu-Co-1 at a reaction temperature of 750 °C.

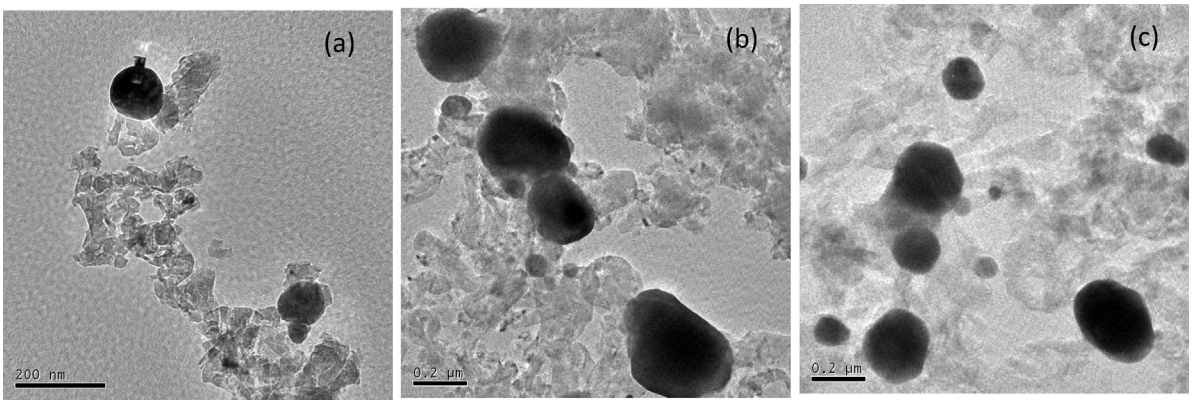

Fig. 13. TEM micrographs of spent catalysts: (a) Ni-Cu-Co-3, (b) Ni-Cu-Co-4, and (c) Ni-Cu-Co-5 at a reaction temperature of 750 °C.

dispersing process in Fig. 12(a). In this case, large spherical alloy particles were formed and no quasi-liquid catalyst particles were observed as shown in Fig. 13. Interplanar distance $d_{(002)}$ and the average coherent scattering region directed perpendicular to the graphite plane (002) (Lc) of the deposited carbon were determined from the XRD data in Fig. 10. Perfect graphite has an interplanar distance between basal planes of 0.3354 nm while interplanar distances of 0.344 nm had been measured in highly disordered turbostratic carbons [50]. As shown in Fig. 10, the structural parameters of the carbon were influenced by the temperature of methane decomposition. Based on the comparison among samples of Ni-Cu-Co-3, Ni-Cu-Co-4 and Ni-Cu-Co-5, which were active for the reaction temperatures of 700 and 750 °C, it could be seen that the higher reaction temperature led to a relatively larger average size of carbon coherent scatting region and a slightly smaller interplanar distance between basal planes which was tending towards to that of the perfect graphite.

To evaluate the effect of reaction temperature on the catalyst, the amount of Co in the alloy is critical. A low Co constituent in the alloy will result in a quasi-liquid state at the required reaction temperature such as the sample Ni-Cu-Co-1 in Fig. 12(a). A high Co constituent can elude the occurrence of the quasi-liquid state and its effects on the catalysis reaction. Based on the results for the spent catalysts in Fig. 12 and Fig. 13, the sample Ni-Cu-Co-3 with the desired Co content was selected to evaluate the effect of temperature on catalyst reaction. At 750 °C, spherical Ni-Cu-Co alloy particles were mostly observed as shown in Fig. 13(a). When the reaction temperature was set at 775 °C, the catalyst transformed itself into a quasi-liquid state and formed CNTs as shown in Fig. 14(a). At 800 °C, elongated liquid-like catalyst particles or smaller split particles (Fig. 14(b) and (c)) were observed which led to abrupt deactivation with the formation of bamboo-like carbon or carbon shells.

4. Discussion

Chesnokov and Chichkan [52] studied the catalytic activity of 70Ni-10Cu-10Fe/Al_2O_3 catalyst for CDM in a rotating reactor. The catalyst was prepared by mechanochemical activation of a mixture of transition metal oxides (Fe_2O_3, NiO, CuO). Their results showed that the addition of Fe to Ni-Cu resulted in enhanced stability of the catalyst. They explained that the diffusion coefficient of carbon atoms through the iron metal is three orders of magnitude higher than through nickel metal. This makes the diffusion of carbon atoms through the bulk of the Ni-Fe-Cu alloy particles faster than through the Ni-Cu alloy particles. However, based on the physicochemical properties of selected transition metals in Table 2, the coefficient of carbon diffusion is higher in nickel than iron, and therefore the enhanced stability of Ni-Fe-Cu catalyst is not due to differences in carbon diffusion rate. The carbon solubility and coefficient of carbon diffusion in some selected transition metals are also given in Table 2. The coefficients of carbon diffusion in the following metals in decreasing order are nickel, iron and cobalt. The carbon solubilities in metal at melting points decrease in the order of iron, cobalt and nickel. Therefore, the effect of iron or cobalt on the catalyst stability of Ni-Fe-Cu or Ni-Cu-Co cannot be ascribed to the differences in carbon diffusion coefficient as carbon diffusion in nickel is higher than in iron and cobalt. It is more reasonable to relate the alloy synergism to the effect due to the melting point. Based on the performance of Ni-Cu-3, Ni-Cu-Co-1, Ni-Cu-Co-2 and Ni-Cu-Co-3 at 750 °C (shown in Fig. 6) and their TEM micrographs (Fig. 12 and Fig. 13), it can be concluded that the addition of cobalt

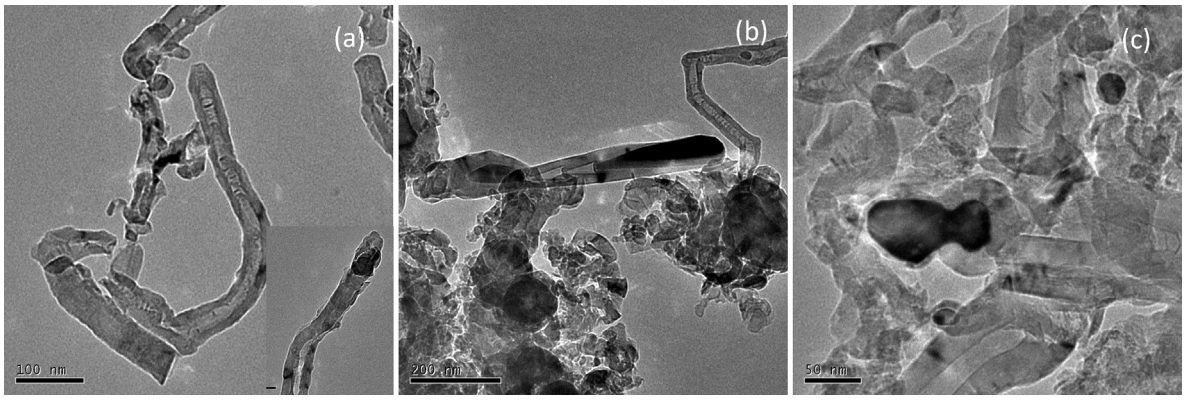

Fig. 14. TEM micrographs of spent catalysts: Ni-Cu-Co-3 at different reaction temperature of (a) 775 °C and (b) and (c) 800 °C.

Table 2
Physico-chemical properties of selected transition metals. NA = data not available [51].

Macroscopic property	Iron	Cobalt	Nickel	Palladium	Copper	Molybdenum
Density, at 20 °C (liquid state) (kg m^{-3})	7874 (7035)	8900 (7670)	8902 (7780)	12020 (10379)	8960 (7940)	10220 (9330)
Melting temperature (T_{melt}) (°C)	1536	1495	1453	1553	1083	2617
Surface tension at 20 °C (at 2000 °C) (N m^{-1})	1.95 (1.72)	2.1 (1.68)	1.86 (1.57)	(2.1) (1.72)	1.75 (0.95)	2.2 (NA)
Equilibrium vapour pressure (at t = 1216 °C) (Pa)	5.5×10^{-3}	4.7×10^{-3}	4.0×10^{-3}	2.1×10^{-2}	7.1×10^{-1}	7.6×10^{-11}
Carbon solubility (at.%) at T_{melt}	20.2	13.9	10.7	~5	2×10^{-4}	60–70
Coefficient of carbon diffusion in metal (m^2 s^{-1}) (at t = 1000 °C)	1.5×10^{-11}	1×10^{-11}	2×10^{-11}	6×10^{-11}	NA	NA

prevents the occurrence of quasi-liquid state in the catalyst. As shown in Table 2, copper has the lowest melting point (among the listed transition metals in the table) at 1083 °C, which is still much higher than the highest reaction temperature in the tests conducted here. In addition, nickel, cobalt and iron have much higher melting point temperatures, which are 1453, 1495 and 1536 °C, respectively. Usually, the alloy will have a melting point which will fall somewhere in between the respective melting points of the constituent metals. The existence of the quasi-liquid-like metal at about 750 °C for the Ni-Cu-Co alloy catalysts in the tests conducted in this study, which is much lower than their respective metal melting temperatures, can only be attributed to the size effect of the metal at nanometre level and the interfacial effect between the carbon and the metal catalyst [34]. A lower melting point will result in the quasi-liquid phenomenon occurring more easily. Therefore, it is reasonable to expect the temperature of the initial occurrence of the quasi-liquid state catalyst to be higher for Ni-Cu-Co than that of Ni-Cu series with the same copper content.

5. Conclusions

A series of unsupported Ni-Cu-Co alloy particles with promising catalytic activity were prepared by thermal decomposition of Ni-Cu-Co oxalates in methane atmosphere. The percent composition of the constituent metals in the Ni-Cu-Co alloy catalyst was a dominant parameter that could affect the catalytic activity of the catalyst. The addition of cobalt led to the formation of alloy particles with smaller crystalline size and particle size than those of Ni-Cu alloy or pure Ni particles. With increasing cobalt content, the catalyst stability at higher temperatures had improved but further continual increase of cobalt content led to phase separation. In general, given the same copper content, the addition of cobalt would improve the stability of the catalyst at a higher reaction temperature such as at 750 °C. This was because cobalt has a higher melting point than nickel and copper, which would therefore delay the occurrence of the quasi-liquid state. However, without nickel, cobalt and copper could not remain in the stable alloy state in the reaction and furthermore, the cobalt particles would be deactivated easily due to carbon encapsulation.

References

[1] T.R. Karl, K.E. Trenberth, Science 302 (2003) 1719–1723.
[2] T.N. Veziroglu, Int. J. Hydrogen Energ. 12 (1987) 99–129.
[3] T.J. Crowley, Science 289 (2000) 270–277.
[4] J.T. Overpeck, J.E. Cole, Ann. Rev. Environ. Resourc. 31 (2006) 1–31.
[5] T.V. Choudhary, C. Sivadinarayana, C.C. Chusuei, A. Klinghoffer, D.W. Goodman, J. Catalysis 199 (2001) 9–18.
[6] Y.D. Li, D.X. Li, G.W. Wang, Catal. Today 162 (2011) 1–48.
[7] J.N. Coleman, U. Khan, W.J. Blau, Y.K. Gun'ko, Carbon 44 (2006) 1624–1652.
[8] M. Moniruzzaman, K.I. Winey, Macromolecules 39 (2006) 5194–5205.
[9] S.R. Bakshi, D. Lahiri, A. Agarwal, Int. Mater. Rev. 55 (2010) 41–64.
[10] X. Liu, M. Wang, S. Zhang, B. Pan, J. Environ. Sci. 25 (2013) 1263–1280.
[11] Z. Yang, H.G. Nie, X. Chen, X.H. Chen, S.M. Huang, J. Power Sources 236 (2013) 238–249.
[12] J. Huang, B.G. Sumpter, V. Meunier, G. Yushin, C. Portet, Y. Gogotsi, J. Mater. Res. 25 (2010) 1525–1531.
[13] N.Z. Muradov, T.N. Veziroglu, Int. J. Hydrogen Energ. 30 (2005) 225–237.
[14] Y. Zhang, K.J. Smith, Catal. Lett. 95 (2004) 7–12.
[15] M.A. Ermakova, D.Y. Ermakov, L.M. Plyasova, G.G. Kuvshinov, Catal. Lett. 62 (1999) 93–97.
[16] M.A. Ermakova, D.Y. Ermakov, G.G. Kuvshinov, Appl. Catal. A-Gen. 201 (2000) 61–70.
[17] S. Takenaka, S. Kobayashi, H. Ogihara, K. Otsuka, J. Catalysis 217 (2003) 79–87.
[18] J.L. Pinilla, I. Suelves, M.J. Lázaro, R. Moliner, J.M. Palacios, Appl. Catal. A: Gen. 363 (2009) 199–207.
[19] H.Y. Wang, A.C. Lua, J. Phys. Chem. C 116 (2012) 26765–26775.
[20] A.C. Dupuis, Prog. Mater. Sci. 50 (2005) 929–961.
[21] J.L. Chen, X.M. Li, Y.D. Li, Y.N. Qin, Chem. Lett. 32 (2003) 424–425.
[22] J. Li, G. Lu, K. Li, W. Wang, J. Mol. Catal. A: Chem. 221 (2004) 105–112.
[23] Y. Li, B. Zhang, X. Tang, Y. Xu, W. Shen, Catal. Commun. 7 (2006) 380–386.
[24] P. Ferreira-Aparicio, I. Rodríguez-Ramos, A. Guerrero-Ruiz, Appl. Catal. A: Gen. 148 (1997) 343–356.
[25] Y. Li, B. Zhang, X. Xie, J. Liu, Y. Xu, W. Shen, J. Catalysis 238 (2006) 412–424.
[26] R.P. Raffaelle, B.J. Landi, J.D. Harris, S.G. Bailey, A.F. Hepp, Mater. Sci. Eng.: B 116 (2005) 233–243.
[27] B.J. Landi, C.D. Cress, C.M. Evans, R.P. Raffaelle, Chem. Mat. 17 (2005) 6819–6834.
[28] C.M. Schauerman, M.J. Ganter, G. Gaustad, C.W. Babbitt, R.P. Raffaelle, B.J. Landi, J. Mater. Chem. 22 (2012) 12008–12015.
[29] F. Valentini, A. Amine, S. Orlanducci, M.L. Terranova, G. Palleschi, Anal. Chem. 75 (2003) 5413–5421.
[30] A. Chambers, T. Nemes, N.M. Rodriguez, R.T.K. Baker, J. Phys. Chem. B 102 (1998) 2251–2258.
[31] A.F. Cunha, J.J.M. Orfal, J.L. Figueiredo, Appl. Catal. A: Gen. 348 (2008) 103–112.
[32] A.C. Lua, H.Y. Wang, Appl. Catal. B: Environ. 132–133 (2013) 469–478.
[33] L.B. Avdeeva, O.V. Goncharova, D.I. Kochubey, V.I. Zaikovskii, L.M. Plyasova, B.N. Novgorodov, S.K. Shaikhutdinov, Appl. Catal. A 141 (1996) 117–129.
[34] Y.D. Li, J.L. Chen, Y.M. Ma, J.B. Zhao, Y.N. Qin, L. Chang, Chem. Commun. (1999) 1141–1142.
[35] T.V. Reshetenko, L.B. Avdeeva, Z.R. Ismagilov, A.L. Chuvilin, V.A. Ushakov, Appl. Catal. A: Gen. 247 (2003) 51–63.
[36] J. Chen, Y. Li, Z. Li, X. Zhang, Appl. Catal. A: Gen. 269 (2004) 179–186.
[37] H.Y. Wang, R.T.K. Baker, J. Phys. Chem. B 108 (2004) 20273–20277.
[38] L. Dussault, J.C. Dupin, C. Guimon, M. Monthioux, N. Latorre, T. Ubieto, E. Romeo, C. Royo, A. Monzon, J. Catalysis 251 (2007) 223–232.
[39] A. Monzon, N. Latorre, T. Ubieto, C. Royo, E. Romeo, J. Villacampa, L. Dussault, J.C. Dupin, C. Guimon, M. Montioux, Catal. Today 116 (2006) 264–270.
[40] Y. Echegoyen, I. Suelves, M.J. Lázaro, R. Moliner, J.M. Palacios, J. Power Sources 169 (2007) 150–157.
[41] J. Ashok, P.S. Reddy, G. Raju, M. Subrahmanyam, A. Venugopal, Energ. Fuel 23 (2009) 5–13.
[42] H.G. Jiang, M. Rühle, E.J. Lavernia, J. Mater. Res. 14 (1999) 549–559.
[43] S. Singh, P. Srivastava, G. Singh, J. Alloy Compd. 562 (2013) 150–155.
[44] B. Bakhit, A. Akbari, JCT Res. 10 (2013) 285–295.
[45] K. Takanabe, K. Nagaoka, K. Nariai, K.I. Aika, J. Catal. 232 (2005) 268–275.
[46] R.-F. Horng, H.-H. Huang, M.-P. Lai, C.-S. Wen, W.-C. Chiu, Int. J. Hydrogen Energ. 33 (2008) 3719–3727.
[47] H. Liu, R. Zhang, R. Yan, B. Wang, K. Xie, Appl. Surf. Sci. 257 (2011) 8955–8964.
[48] M. Kumar, Y. Ando, J. Nanosci. Nanotechnol. 10 (2010) 3739–3758.
[49] N. Latorre, F. Cazana, V. Martinez-Hansen, C. Royo, E. Romeo, A. Monzon, Catal. Today 172 (2011) 143–151.
[50] H. Fujimoto, Carbon 41 (2003) 1585–1592.
[51] A. Moisala, A.G. Nasibulin, E.I. Kauppinen, J. Phys.-Condensed Matter 15 (2003) S3011–S3035.
[52] V.V. Chesnokov, A.S. Chichkan, Int. J. Hydrogen Energ. 34 (2009) 2979–2985.